Segmentation of Brain MR Images Through a Hidden Markov Random Field Model and the Expectation-Maximization Algorithm

Tanya Nair
McGill University
Montreal, QC
tnair@cim.mcgill.ca

Abstract

Markov Random Fields (MRFs) are a powerful statistical tool that are exploited in the field of brain tissue segmentation to provide spatial context into generative models. Existing work has used MRFs as priors in finite mixture models in order to model tissue intensities, but as Zhang et al. *stress in [8], the use of finite models is rooted in mathematical convenience as opposed to a statistical foundation. Using a hidden MRF to model tissue intensities avoids these assumptions. This paper describes an implementation of the Hidden MRF model optimized with Expectation Maximization (EM) as described Zhang* et al. *in [8] to segment brain tissues from the OASIS cross-sectional brains dataset, and discusses the strengths and weaknesses of this model in this context.*

1. Introduction

Tissue segmentation and classification is a pressing challenge within the field of medical imaging. The ability to precisely classify tissues allows for quantitative analyses of substructures that are correlated with disease evolution. For example, Alzheimer's Disease can be characterized by atrophy in otherwise healthy white matter and gray matter brain tissue.

When examining tissue in the brain, Magnetic Resonance Imaging (MRI) is the predominant imaging technique of choice as it is non-invasive and provides excellent soft tissue contrast. Additionally, advances in MRI technology have enabled the acquisition of high resolution images across different modalities that provide differing contrasts for sub-tissue categories. Alongside these advances come the need for automated methods to reduce the time and economic costs associated with manual segmentation (which is performed by expertly trained radiologists). Automated techniques can also address inter and intra-human error that persists despite standardized protocols and training procedures.

Automated brain MR tissue segmentation is a non-trivial problem for a number of reasons. Non-homogeneities induced by the scanning technology limit the efficacy of intensity based classifiers; multi-modal information from different scan procedures has to be aggregated; and when segmenting pathology, the non-deterministic size, shape, and location of abnormalities provide additional challenges. Integrating local context into tissue classification models is one tool used to overcome some of these challenges. For this reason, Markov Random Fields (MRFs) have been widely used in the literature. MRFs integrate spatial information into the segmentation process in a probabilistic way such that the classification of a voxel becomes statistically dependent on its neighbouring pixels.

MRF models applied to brain MR segmentation prior to the work of Zhang *et al*. had two key limitations [8]. They either did not have a parameter fitting step (as in [3]), or the parameter estimation step was limited by the finite mixture model being employed. These models, such as the Gaussian Mixture Model in [7], are employed as mathematically convenient approximations, which are not statistically grounded. Furthermore, finite models operate best under low noise conditions, which is a poor assumption in real MR images where bias fields and partial volume effects distort within-class voxel intensities. This is pointed out by Zhang *et al*. in [8], who are thus motivated to develop a hidden MRF (HMRF) to model tissue intensities. Using a HMRF allows for the integration of spatial dependences into the tissue intensity model (which were previously modelled separately). A hidden Markov model is a statistical process generated by a Markov chain where the state (ie. tissue class) is not observable, but the output (ie. voxel intensity) is observed and is probabilistically conditioned on the input state. In [8] this concept is extended to a 3D HMRF whereby the source is a MRF describing the voxel intensities in the brain image. The authors use a Gaussian distribution to describe the observed random field, and use Expectation-Maximization (EM) to fit their HMRF

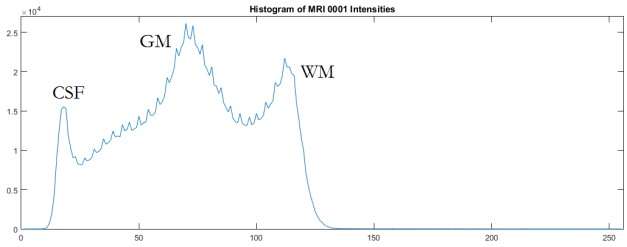

Figure 1. Intensity Histogram of Subject 0001 MR-T1 Image

model parameters on simulated images of non-diseased tissue to segment white matter (WM), gray matter (GM), and cerebrospinal fluid (CSF).

This paper describes the high level segmentation pipeline, followed by the mathematical modelling of the HMRF, the optimization through EM, as well as an implementation of the model applied to WM, GM, CSF segmentation of 416 brains in the OASIS cross-sectional dataset. Experimental results are given characterizing the performance against the FAST-FSL implementation, followed by a discussion of the strengths and weaknesses of the model.

2. Model Description

For each image, an initial segmentation is performed using Otsu thresholding. With this initial segmentation, the HMRF model parameters are calculated for each tissue class (GM/WM/CSF). These parameters are fed into an EM routine which iteratively calculates MRF-MAP tissue labels for each voxel, and then (in the maximization step), updates the HMRF mean, and variance parameters for each class. This continues until the EM stopping criteria has been met.

2.1. Initial Segmentation

Because EM guarantees convergence to a local optimum, the initial segmentation is a critical stage of the algorithm. Zhang *et al*. employ Otsu thresholding as described in [6] to obtain the initial segmentation. Otsu thresholding seeks to find the thresholds that minimize intra-class (within-class) variance. The core underlying assumption is that the intensity histogram of the image will follow a trimodal distribution, which as shown in Figure 2.1 is upheld.

2.2. HMRF Model

2.2.1 MRF Theory

This section reviews the set of notation and design features that dictate how an MRF model operates. As described in [4], a neighbourhood system N over the set of sites S is defined as $\mathcal{N} = \{\mathcal{N}_i | i \in S\}$. In imaging applications, a site is generally interpreted as a pixel or voxel. A site cannot be a neighbour to itself, and the neighbourhood definition is mutual. The set of sites S can further be constrained if they are described as a regular lattice, and the neighbourhood is subsequently defined as the subset of sites that lie within a given radius. In [8], the authors use a 3D first-order neighbourhood, with 6 neighbours for each image voxel.

With this definition of a neighbourhood, a clique is then defined as a site, pair, triple, etc. of neighbouring voxels. In [8], the maximum clique size is two. Given a neighbourhood system $\mathcal{N}$, X is a MRF on the sites in S if and only if the following conditions of positivity and Markovianity are met:

$$P(x) > 0, x \in \mathcal{X} \tag{1}$$

$$P(x_i | x_{S-i}) = P(x_i | x_{N_i}) \tag{2}$$

As per the Hammersley-Clifford theorem ([2]), a MRF can equivalently be written as a Gibbs distribution as follows

$$P(x) = \frac{exp(-U(x))}{Z} \tag{3}$$

where Z is a normalizing constant and $U(x)$ is an energy function defined by a sum of clique potentials $V_c(x)$ over all cliques as follows

$$U(x) = \sum_{c \in C} V_c(x) \tag{4}$$

In [8], the authors use the Dirac delta function to form the clique potentials as in Equation 5. The neighbourhood field is further constrained to be homogeneous, in-plane isotropic, and out-of-plane anisotropic neighbourhood system. Homogeneity ensures the potential function is independent of the location across the MRF sites. The in-plane isotropy, and out-of-plane anisotropy is a consequence of the MRI acquisition that results in voxel resolutions of $1x1x3mm^3$ in the (x, y, z) directions.

$$V_c(x) = \delta(x_i - x_j) \tag{5}$$

2.2.2 HMRF Theory

The hidden Markov model (HMM) is the 1-dimensional counterpart to the HMRF. A HMM is a stochastic process generated by a Markov Chain consisting of a set of latent ('hidden') states S, a set of observations O, state transition probabilities that describe how one states move to another (Equation 6), and observation emission probabilities that govern what the observed data is given a hidden state (Equation 7). As the name suggests, the chain is Markovian in that a future state is independent of past states given the present state (Equation 8).

$$P(S_{t+1} = s' | S_t = s) \tag{6}$$

$$P(O_t = o|S_t = s) \tag{7}$$

$$P(S_{t+2}|S_{t+1}, S_t) = P(S_{t+2}|S_{t+1}) \tag{8}$$

In the 2D extension, hidden Mark Random Fields are analagous to the previously defined hidden states. The hidden field can be interpreted as the tissue class labels and the observed field can be interpreted as the MR image intensity values. In [8], the authors use a Gaussian emission distribution that describes the observed field, parameterized by the intensity value and the parameters associated with the tissue class label as follows

$$P(y_i|x_{N_i}, \theta) = \sum_{l \in L} \mathcal{N}(y_i; \theta_l) p(l|x_{N_i}) \tag{9}$$

where i is a given pixel, x_{N_i} are the labels for the neighbouring pixels, l is a label class index.

2.3. MRF-MAP Classification

With a HMRF model that links the pixel intensities to their hidden class labels, MRF-MAP estimation is performed to obtain an estimate of the labels $\hat{\boldsymbol{x}}$ according to the maximum a posterior criteria given in Equation 10. The arguments of the product in this equation can equivalently be written as Gibbs distributions according to the Hammersley-Clifford Theorem [2]. Consequently, Equation 10 can be equivalently be written and simplified using Equation 3 as follows

$$\hat{x}_{MAP} = argmax_{x \in X}\{P(y|x)P(x)\} \tag{10}$$

$$P(x) = \frac{exp(-U(x))}{Z} \quad P(y|x) = \frac{exp(-U(y|x))}{Z'} \tag{11}$$

$$\hat{x}_{MAP} = argmin_{x \in X}\{U(y|x) + U(x)\} \tag{12}$$

where $U(\cdot)$ is the energy function (described further in the previous section), and Z, Z' are normalization constants. This result can be interpreted as follows: minimize the posterior energy in order to obtain label estimates.

2.3.1 Minimization of Posterior Energy

As there is no closed-form solution to Equation 12, Iterated Conditional Modes (ICM) is used to search for a local minima of the energy. ICM is a deterministic, iterative algorithm that performs a greedy (local) optimization. In each iteration, each voxels label is updated by minimizing the posterior energy as per the following update algorithm

$$x_i^{t+1} \leftarrow argmin_{x_i} U(x_i|y_i, x_{N_i}) \tag{13}$$

2.4. Maximum Likelihood Parameter Updates

With the MRF-MAP labels, the following stage is the Maximization stage of the EM algorithm. Here, maximum likelihood parameter estimates are obtained for the MRF model. Because the Gaussian distribution was chosen to represent the emission probabilities, the model parameters of the mean and variance for each tissue class using an update of the data log-likelihood. The update equations for the log-likelihood $P(l|y_i)$, mean μ, and variances σ^2 at iteration t, pixel i, and class l are given in Equations 14 - 16.

$$P^t(l|y_i) = \frac{\mathcal{N}(y_i; \theta_l) p(l|x_{N_i})}{p(y_i)} \tag{14}$$

$$\mu_l^{t+1} = \frac{\sum_{i \in S} P^t(l|y_i) y_i}{\sum_{i \in S} P^t(l|y_i)} \tag{15}$$

$$(\sigma_l^{t+1})^2 = \frac{\sum_{i \in S} P^t(l|y_i)(y_i - \mu_l^{t+1})^2}{\sum_{i \in S} P^t(l|y_i)} \tag{16}$$

These equations follow from the derivations in [8].

3. Experimental Implementation

For this project, a full implementation was completed for the 3D HMRF, MRF-MAP estimation with ICM, and optimization using EM. Code implementing the Otsu thresholding was sourced, and initialization with Otsu thresholding and kmeans was compared. The model was tested on the OASIS cross-sectional dataset, a public dataset consisting of 416 normal and early-onset Alzheimer's Disease subjects. For each subject, a brain masked MR-T1 image that is bias-field registered to the Talairach and Tournoux 1988 atlas ([1]) is provided. Ground truth segmentations using the FAST-FSL implementation of the algorithm by Zhang *et al*. are also provided for each image. Details of the acquisition protocol and preprocessing steps can be found in [5]. DICE (overlap ratio), sensitivity (true positive), and specificity (true negative) scores are calculated for each tissue class in each image and averaged across the dataset to form the results in Table 1.

4. Results

Qualitative results comparing ground truth, initial segmentation, and the final HMRF segmentation are shown in Figures 2-7. The two figures contrast two different initializations (Otsu and kmeans). Quantitative results are provided in Table 1. The full algorithm takes approximately 30 seconds to run on each 7929856-voxel image in an Intel Core i7 3.4 GHz system with 32 GB of RAM.

5. Discussion

Quantitatively it is observed that the Otsu thresholding outperforms the kmeans initialization in the CSF, but the

Table 1. Initial and Final Segmentation Scores for Otsu and kmeans Initialization

		CSF			Grey Matter			White Matter		
		DICE	Sensitivity	Specificity	DICE	Sensitivity	Specificity	DICE	Sensitivity	Specificity
Initial Score	Otsu	0.5255	0.3615	1.0000	0.7650	0.7919	0.9619	0.8670	0.9977	0.9729
	Kmeans	0.5255	0.3615	1.0000	0.7650	0.7919	0.9619	0.8670	0.9977	0.9729
Final Score	Otsu	0.6918	0.5718	0.9975	0.8389	0.8720	0.9732	0.9149	0.9822	0.9854
	Kmeans	0.6446	0.5093	0.9984	0.8458	0.9066	0.9681	0.9252	0.9670	0.9891
% change	Otsu	31.64%	58.21%	-0.25%	9.66%	10.11%	1.18%	5.53%	-1.55%	1.28%
	Kmeans	22.65%	40.91%	-0.16%	10.56%	14.48%	0.64%	6.71%	-3.08%	1.66%

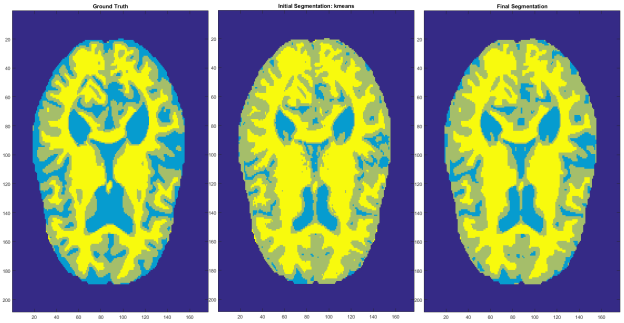

Figure 2. Initial Segmentation with Kmeans and Final Segmentation Results (Slice 81, Subj 0001)

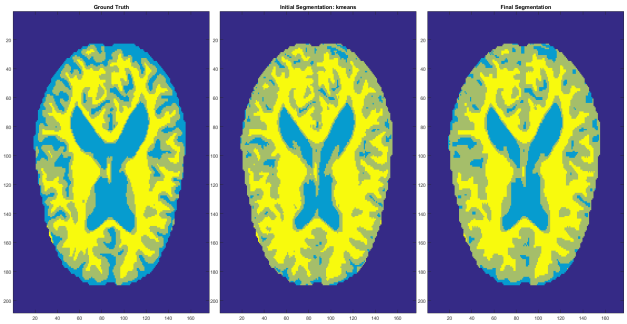

Figure 3. Initial Segmentation with Kmeans and Final Segmentation Results (Slice 90, Subj 0001)

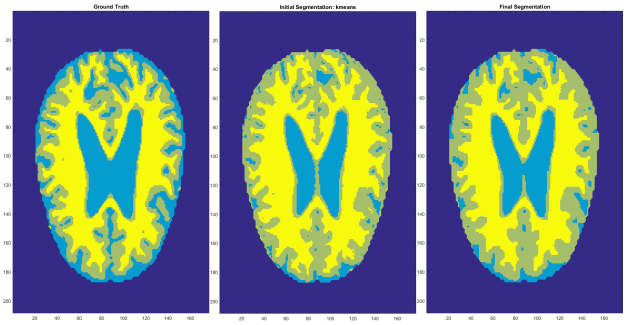

Figure 4. Initial Segmentation with Kmeans and Final Segmentation Results (Slice 100, Subj 0001)

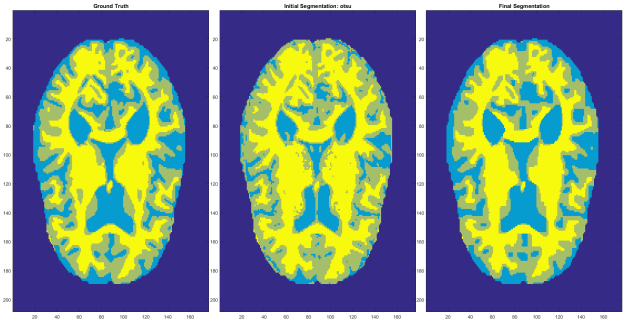

Figure 5. Initial Segmentation with Otsu and Final Segmentation Results (Slice 81, Subj 0001)

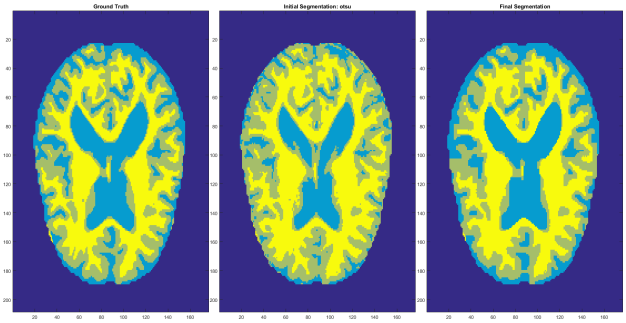

Figure 6. Initial Segmentation with Otsu and Final Segmentation Results (Slice 90, Subj 0001)

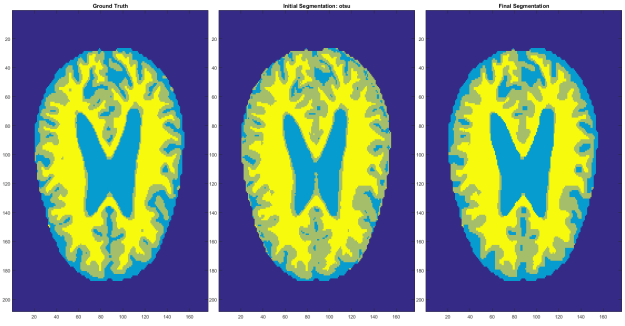

Figure 7. Initial Segmentation with Otsu and Final Segmentation Results (Slice 100, Subj 0001)

converse is true for the WM and GM tissues. This is reflected in the qualitative results where the final segmentation initialized with Otsu is significantly better at segmenting the CSF. This result is a bit surprising considering how similar the Otsu and kmeans initial segmentations are, although it may result from the hyperparameter optimization that was kept fixed between the two methods.

It should be noted that the metric of 'ground truth' is not

a manual segmentation but the FAST-FSL implementation of the algorithm, and consequently the results should be interpreted as a measure of similarity to a correct implementation of [8], as opposed to a perfect segmentation. As evident in Table 1, this implementation of the HMRF-EM framework to the brain segmentation task provides adequate results, but falls short of the FAST-FSL implementation. This shortcoming can be significantly attributed to the initial segmentation. In this project the initial segmentation was completed with Otsu thresholding and kmeans, which provided similar results. If a tissue stucture was smoothed over in this initialization, the HMRF is unable to recover it. This is demonstrated in Figures 2 and 5 where there is oversmoothing in the white matter close to the ventricles. Furthermore, these methods are unstable: 9% of the images failed to converge to a plausable solution (ie. one class was reduced to 0 instances). This could be resolved by using a Bayesian method of initializing. A Bayesian method of initializing would take the mean and variance class parameters obtained through Otsu thresholding to obtain Maximum Likelihood estimation; this can be explored in future work. Another contributor to this implementations shortcoming is the lack of bias field modelling. In [8], the authors model the bias field in order to correct for intensity inhomogeneities in the MR images and this is a part of the FAST-FSL implementation. Although the images in the OASIS dataset used for this project are bias field corrected with either N3 or N4 normalization, the integration of the model into the HRMF would provide improved results.

Despite the shortcomings of initialization and bias field estimation, the results showcase the ability of the implemented HMRF-EM to converge to a result that improves the initial segmentation. An advantage of this model over finite-mixture models is the explicit embedding of spatial relations into the intensity model, which makes the HMRF more robust to noise than the model in [7]. Furthermore, this HMRF-EM framework is modular (the bias field modelling in [8] is an example of this), does not require any training data, and is fully automated.

6. Conclusion

In this paper, an implementation of the HMRF-EM as described in [8] is presented with the application to segment 3D brain MR images from the OASIS cross-sectional dataset. The results obtained measured a shortcoming of the project implementation to the FAST-FSL implementation of the author's work which is attributed primarily to the initial segmentation and the bias field modelling.

References

[1] R. L. Buckner, D. Head, J. Parker, A. F. Fotenos, D. Marcus, J. C. Morris, and A. Z. Snyder. A unified approach for morphometric and functional data analysis in young, old, and demented adults using automated atlas-based head size normalization: reliability and validation against manual measurement of total intracranial volume. *Neuroimage*, 23(2):724–738, 2004.

[2] J. M. Hammersley and P. Clifford. Markov fields on finite graphs and lattices. 1971.

[3] K. Held, E. Kops, B. Krause, W. Wells, R. Kikinis, and H.-W. Muller-Gartner. Markov random field segmentation of brain mr images. *Medical Imaging, IEEE Transactions on*, 16(6):878–886, Dec 1997.

[4] S. Z. Li. *Markov random field modeling in image analysis*. Springer Science & Business Media, 2009.

[5] D. S. Marcus, T. H. Wang, J. Parker, J. G. Csernansky, J. C. Morris, and R. L. Buckner. Open access series of imaging studies (oasis): cross-sectional mri data in young, middle aged, nondemented, and demented older adults. *Journal of cognitive neuroscience*, 19(9):1498–1507, 2007.

[6] N. Otsu. A threshold selection method from gray-level histograms. *Automatica*, 11(285-296):23–27, 1975.

[7] K. Van Leemput, F. Maes, D. Vandermeulen, and P. Suetens. Automated model-based tissue classification of mr images of the brain. *Medical Imaging, IEEE Transactions on*, 18(10):897–908, Oct 1999.

[8] Y. Zhang, M. Brady, and S. Smith. Segmentation of brain mr images through a hidden markov random field model and the expectation-maximization algorithm. *Medical Imaging, IEEE Transactions on*, 20(1):45–57, Jan 2001.